Alexandrov RESEARCH INSTITUTE OF TECHNOLOGY
N I T I

Phase diagrams for multicomponent systems containing corium and products of its interaction with NPP materials (CORPHAD) Phase 2

INVESTIGATION OF TERNARY OXIDIC SYSTEMS: SYSTEM UO_x – ZrO_2 – FeO_y

---

PROGRESS REPORT

01/07/03 – 25/02/05

Project title	Phase diagrams for multicomponent systems containing corium and products of its interaction with NPP materials (CORPHAD, №1950.2)
Customer	ISTC
File specification	CORPHAD/RCP-0502
Place of project implementation	FGUP Alexandrov Research Institute of Technology (NITI) of the Russian Federal Agency for Atomic Energy Russia 188540, Sosnovy Bor of Leningrad Oblast, NITI
Project manager Name	Yu. N. Aniskievich
Signature	
Date	February, 2005

Authors

Prof. V.B. Khabensky

Dr. S.V. Bechta

Dr. V.S. Granovsky

Prof. V.V. Gusarov

V.I. Almiashev

S.A. Vitol

E.V. Krushinov

Prof. Yu.B. Petrov

Dr. S.Yu. Kotova

Dr. A.A. Sulatsky

Dr. I.V. Kulaghin

Dr. D.B. Lopukh

Dr. A.Yu. Petchenkov

Dr. L.P. Mezentseva

V.G. Blizniuk

V.R. Bulighin

E.M. Beliaeva

E.K. Kaliago

N.E. Kamensky

A.V. Lisenko

A.P. Martynov

V.V. Martynov

E.V. Shevchenko

A.A. Chertkov

S.K. Kutchaeva

N.A. Lomanova

V.F. Popova

CONTENTS

Introduction

The current work is carried out within the ISTC CORPHAD Project in order to specify phase diagrams of corium-based systems and products of its interaction with NPP materials. The reported part of the project deals with the experimental studies of the UO_x – ZrO_2 – FeO_y phase diagram

It should be noted that the UO_x – ZrO_2 – FeO_y system is essential for describing phenomena, which take place during a severe accident.

Fig. 1 shows the concentration domains of the composition typical for the in- and ex-vessel coria (atomic ratio U/Zr=0.8-1.3, FeO_y ~ 30 mass.%). In order to optimize the database on corium phase diagrams, to forecast the behavior of corium interacting with materials containing iron, zirconium and their oxides and understand processes taking place at the corium crystallization, it is important to know ternary eutectic point and final solubility of components, if the system contains solid solutions.

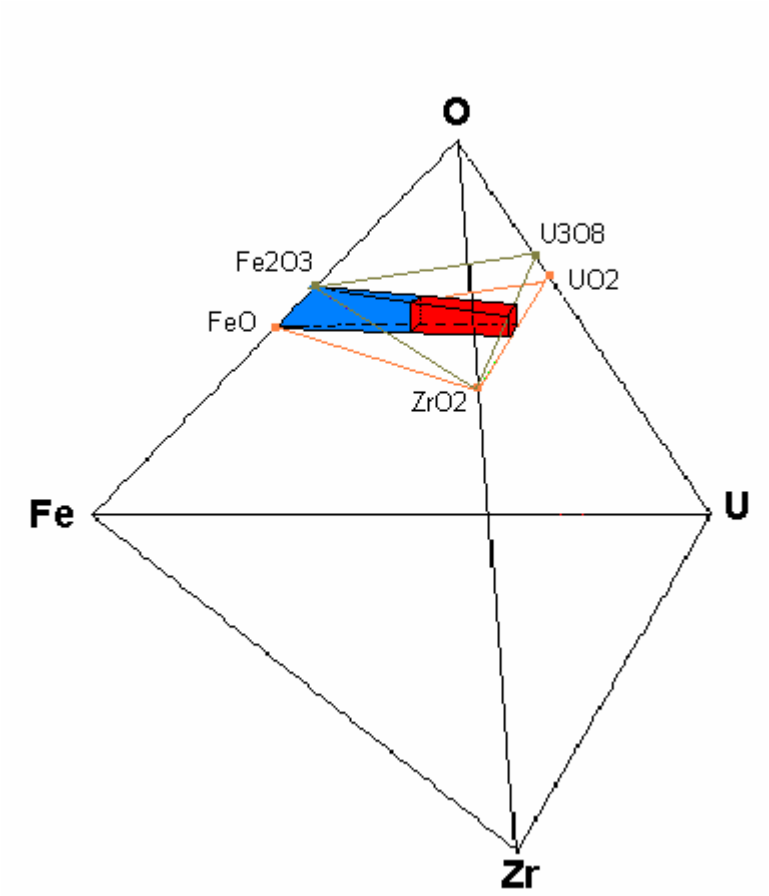

Fig. 1. Concentration domains of the composition typical for the in- and ex-vessel coria

The published data on the considered system are limited. Phase equilibria in this system have been studied in the narrow concentration range within the CIT project [1], also in the ISTC Project #64 "Design of a nuclear reactor core melt catcher on the basis of zirconia concrete". Two domains of the diagram are important in terms of reactor application: the one with low oxygen potential characterizing melt condition at oxygen deficit, another – for fully oxidized corium.

During the first stage of CORPHAD [2] we studied quasibinary systems of UO_2 – FeO and ZrO_2 – FeO at a low oxygen potential.

Previously different authors have studied the same systems in air, so there is some information available on them in [3, 4].

Phase diagram $UO_2 – ZrO_2$ has been studied in details. It is known that at high temperatures its components have unlimited solubility in each other. But when the temperature goes down to ~ 1600°C, the solubility becomes limited and exists only within narrow concentration ranges [5].

The numeric predictions of the $UO_x – ZrO_2 – FeO_y$ ternary eutectics for low oxygen potential and experimental results in air [6] provided different concentration domains of the ternary eutectic point.

The report presents the description and main results of the tests, in which $UO_x – ZrO_2 – FeO_y$ system was investigated both in inert atmosphere and in air, and the ternary eutectic temperature and composition were determined. The experiments have been performed in NITI, Sosnovy Bor and in ISC of RAS, St. Petersburg.

The following experimental objectives were set:

- Determine melting temperature and composition of ternary eutectics in air and inert atmosphere.
- Determine final solubility of components.

1. Experimental setup and methodology

The experiments were conducted on the RASPLAV-3 test facility, which is based on the method of induction melting in a cold crucible (IMCC). The furnace schematics is presented in Fig. 2.

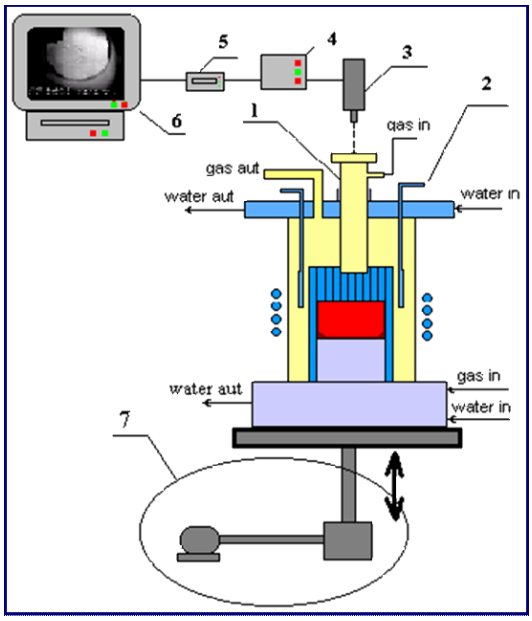

1-pyrometer shaft, 2- adjustable water-cooled electromagnetic screen, 3- pyrometer combined with video camera, 4- MDAS, 5- device for inserting measurement results into video-frames, 6- monitor/video recorder, 7- drive for vertical crucible movement

Fig. 2. Furnace schematics

The molten pool surface was monitored using the video recording system ((5) in Fig.2) combined with pyrometer (3). The system provided 50 Hz frequency inserts of measured temperatures and position of pyrometer sighting spot into each frame of the recording performed with camera (3) and recorder (6). Temperature on the melt surface was measured with a spectral ratio pyrometer RAYTEK MR1-SC. A video camera recorded the surface region within the pyrometer shaft, the diameter of which was 22 mm. The pyrometer sighting spot was ~ 6 mm. The inner diameter of the cold crucible was 38 mm. A ring-shaped region along the crucible wall remained unobserved.

Sampling was performed to determine the initial melt composition. After that the surface of the superheated molten pool was locally cooled, and liquidus temperature of the melt was measured. This was performed by using the water-cooled electromagnetic screen (Fig. 2, (2)), which was moved along the vertical axis of the crucible, its positioning against the previously superheated pool ensured the temperature decrease only in a thin surface layer and did not cause changes in the melt composition. The method of visual polythermal analysis (VPA IMCC) is explained in detail in [7].

An ingot having eutectic composition was produced by the melt crystallization in close-to-equilibrium conditions, by slow (5-10 mm/h) uninterrupted movement of the crucible with melt versus the inductor using the vertical drive (Fig. 2, (7)). When such technique is used, the last to crystallize is the most fusible liquid, i.e. a liquid having the eutectic composition. The physico-chemical analysis of samples from the last-to-crystallize ingot region enables to determine the eutectic composition. Samples from this region were also used for the eutectic temperature determination by the differential-thermal analysis (DTA).

After the above-mentioned studies an approximate composition and temperature of ternary eutectics were determined. This was followed by additional experiments, in which the composition of the initial charge corresponded to the approximate eutectic composition, and the procedure repeated previous experiments. In this way, a large eutectic region was formed during crystallization, and the physico-chemical analysis of samples from this region enabled to determine eutectic composition with an error of 1-2 mass.%.

2. VPA IMCC studies. Experiments CORD 25-27, 31

2.1. Analysis of charge materials

Before the experiments the charge components, UO_2 and FeO (II) were analyzed for the content of basic substance and admixtures.

The content of metallic iron Fe^0 was determined by the copper-sulfate method [8, 9].

The content of Fe(II) and Fe(III) was determined by the photocolorimetry with orthophenanthroline [10-12].

Thermogravimetry was used for determining the O/U ratio in the uranium dioxide powder, it was 2.0 in experiments CORD 25, 26, 31 and 2.24 in case of CORD27 [13]. Uranium dioxide having O/U ratio of 2.24 was introduced into the charge for faster establishment of equilibrium between the melt and gas atmosphere at the partial oxygen pressure of 0.21 atm.

Table 1 presents the data on charge components.

Table 1. Composition of charge components

Components	Content of basic substance, %	Admixtures, mass %	Source
UO_2 powder with particle size <200μm	>99.0	Fe<0.03; As<0.0003; CuO<0.01; phosphates<0.002; chlorides<0.003.	Certificate data, thermogravimetry
$UO_{2.24}$ powder with particle size <50 μm	>99.0	Fe<0.03; As<0.0003; CuO<0.01; phosphates <0.002; chlorides <0.003.	Certificate data, thermogravimetry
ZrO_2 powder with particle size <100 μm	(ZrO_2+HfO_2) >99.3	Al_2O_3<0.03; Fe_2O_3<0.05; CaO<0.03; MgO<0.02; SiO_2<0.2; TiO_2<0.1; P_2O_5<0.15; (Na_2O+K_2O)<0.02.	Certificate data
FeO	67.68	Fe_2O_3-30.86; Fe-0.57	Chemical analysis
Fe_2O_3	>98.1	Sulfates <0.4; Cu<0.006; (K+Na)<0.032; (Ca+Mg)<0.068; Si<0.04; N<0.001	Certificate data
Fe	>99.9	Si-0.0005; Mg-0.0001; Cu-0.0001; Ni-0.019; Pb-0.0001; Zn-0.00028	Certificate data

2.2. Thermodynamic modeling and specification of experiments

Four experiments have been conducted within this part of the project; their specification is presented in Table 2. The experiments were preceded by the thermodynamic calculations of the ternary eutectics composition for the studied system in air and inert atmosphere.

UO_2–ZrO_2–FeO system in the inert atmosphere

The prediction (Fig. 3) was made using the available data on the systems, binary eutectics of which had been previously determined [7, 14].

The initial charge composition was prepared, which corresponded to the primary crystallization zone of FeO. The crystallization of a melt having such composition starts from the refractory component (i.e. FeO. Then the figurative point (Fig. 3) is crossing the line of binary eutectics and joint crystallization of FeO and $(U,Zr)O_2$ solid solution starts. During this eutectic type crystallization the composition shifts along the binary eutectic curve to the ternary eutectic. The ternary eutectic is the last to crystallize. In this way, the experiment is aimed at getting the nucleus of ternary eutectic, which had to be separated from the rest of the ingot and studied using the methods of DTA, VPA in Galakhov microfurnace and SEM/EDX for the exact determination of eutectic composition and temperature.

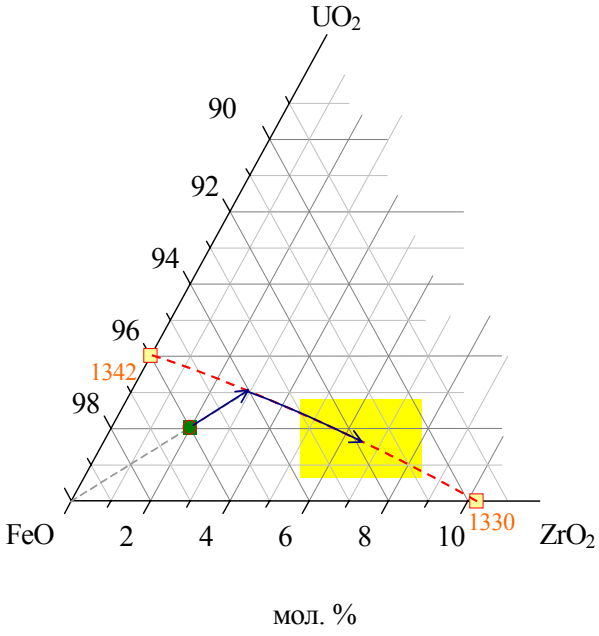

Fig. 3. Predicted composition range of ternary eutectic (yellow): point in the diagram is the composition of initial charge; - - - – predicted curve of binary eutectics; 1342 and 1330°C – temperatures of binary eutectics in UO_2 – FeO and ZrO_2-FeO systems correspondingly

UO_{2+x}–ZrO_2–FeO_y system in air

The composition of ternary eutectics for this system in air (Fig. 4) was predicted using the data on the binary eutectic compositions taken from reference books [15, 4].

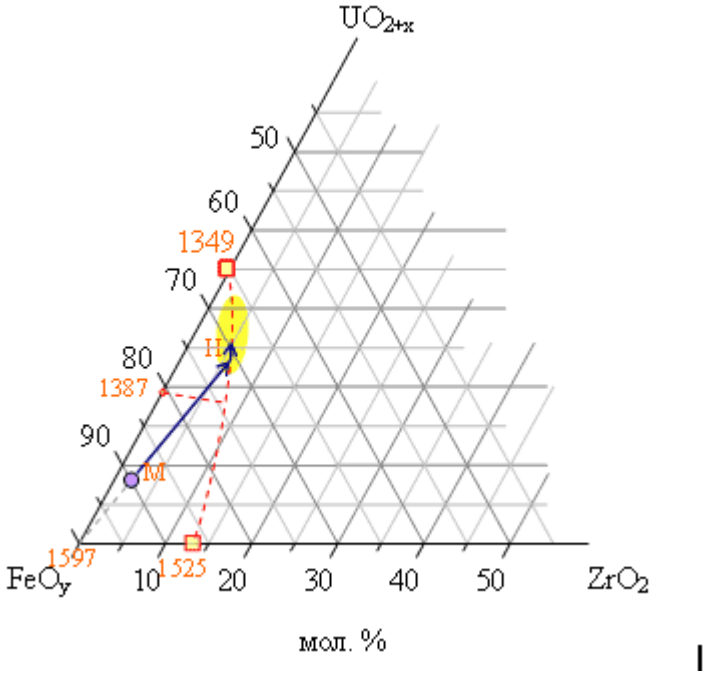

Fig. 4. Predicted composition range of ternary eutectic (yellow): point in the diagram is the composition of initial charge; - - - – predicted curve of binary eutectics; 1349 and 1525°C - temperatures of binary eutectics in UO_{2+x} – FeO_y and ZrO_2-FeO_y systems correspondingly; M – domain of Fe_3O_4 having magnetite structure; H – domain of Fe_2O_3 having hematite structure

Experiments in air have the following specific feature: the crystallization of melt containing iron oxides is accompanied by an additional phenomena - Fe_3O_4 interacts with oxygen to produce Fe_2O_3. For pure substances the temperature, at which Fe_3O_4 oxidizes to Fe_2O_3, is 1387°C, but as the complete conversion kinetics is unknown, the melt was maintained below this temperature for about 1-2 hours in order to establish chemical equilibrium.

The initial charge composition was prepared to be in the domain of Fe_3O_4 primary crystallization. Table 2 gives the specification of experiments.

Table 2. Specification of experiments CORD 25, 26, 27, 31

CORD	Composition, mass.% /mole%							Charge mass, g.	Atmosphere
	UO_2	$UO_{2.24}$	ZrO_2	Fe	Getter (Fe)	FeO	Fe_2O_3		
25	6.8/1.9	-	2.9/1.8	9.0/11.9	1.0/1.3	80.3/83.1	-	287.2	Air
26	22.5/14.1	-	2.5/3.4	1.7/5.0	-	-	73.3/77.4	300.0	
27[1)]	-	58.6/42.3	1.9/3.1	2.4/8.6	-	-	37.1/45.9	332.6	
31[2)]	21.1/6.7	-	6.8/4.7	6.6/10.1	1.0/1.5	64.5/77.0	-	304.7	Ar

[1)]- Initial composition of the charge for this experiment was determined using the results of CORD26 (in air)
[2)]- Initial composition of the charge for this experiment was determined using the results of CORD25 (in the inert atmosphere).

2.3. Experimental procedures

All experimental procedures were similar; they are briefly described in tables 3-6.

Table 3. Experimental procedure of CORD25 in the inert atmosphere

Time from the test start, s	Stage/experimental activity
-300-0	Prestart furnace blowing with argon; flow rate 10 l/min.
0-905	Startup heating, molten pool formation; measurement of its depth (~ 50 mm) and bottom crust (~ 2 mm). Temperature of the molten pool surface ~ 1412ºC.
905-1650	Movement of electromagnetic screen, liquidus temperature is measured three times by the VPA IMCC (Fig. 5, T_{liq} =1348ºC), melt sample is taken.
1650-2420	Melt exposition, crucible is moved downwards (~ 10 mm.) until the generator reacts to the change of position (anode current changes).[1)]
2570-23170	The drive for the vertical movement of the crucible is turned on (speed of 9 mm/h.
23171	HF heating is disconnected. Ingot is crystallized in argon and cooled down. Temperature of the last uncrystallized liquid measured by pyrometer is ~1330ºC.

[1)] – Crystallization indicator in the IMCC conditions is the reduction of the anode current from the generator lamp. To exclude the uncrystallized ingot extraction the preliminary change of crucible position versus inductor was performed.

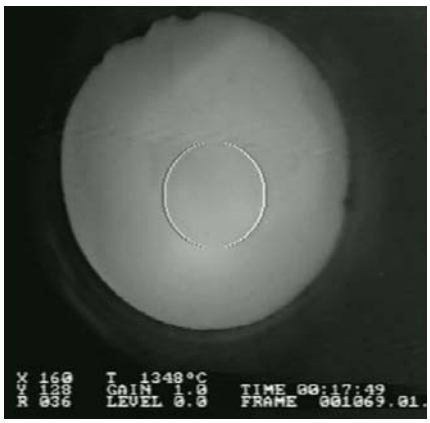

Fig. 5. Video image of the melt surface during the liquidus temperature measurements

Table 4. Experimental procedure of CORD26 in air

Time from the test start, s	Stage/experimental activity
0-1093	Startup heating, molten pool formation; measurement of its depth (~ 40 mm) and bottom crust (~ 2 mm). Temperature of the molten pool surface ~ 1630ºC.
1093-2800	Electromagnetic screen is moved, liquidus temperature is measured three times by the VPA IMCC (Fig. 6, T_{liq} =1537°C), melt sample is taken.
2800-2914	Melt exposition, crucible is moved downwards (~14 mm) until the generator reacts to the change of position (anode current changes).
2977-10490	The drive for the vertical movement of the crucible is turned on (9 mm/h).
10490	The drive for the vertical movement of the crucible is turned off.
10500-12300	The remaining melt is exposed to the temperature of ~1400ºC for its saturation with oxygen.
12300-13500	The drive for the vertical movement of the crucible is turned on (9 mm/h).
13506	HF heating is disconnected. Ingot is crystallized and cooled down.

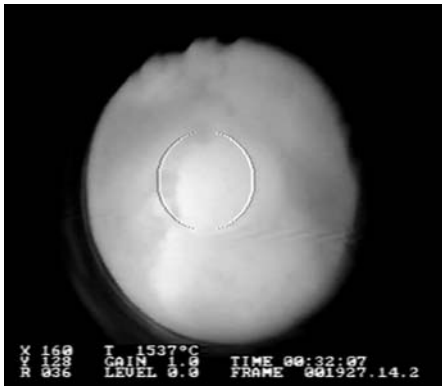

Fig. 6. Video image of the melt surface during the liquidus temperature measurements

In accordance with experimental specifications the surface temperature of initial melt was

1630°C. At this temperature in air Fe_2O_3 loses much oxygen. The attempts to reduce the surface temperature by decreasing power deposition in the melt resulted in the melt crystallization on the molten pool bottom. For this reason the ingot extraction was started at a high temperature of the molten pool. Temperature of the last observed liquid was ~1400°C. For this reason during the melt exposition in air in order to saturate it with oxygen a temperature necessary for Fe_3O_4 conversion into Fe_2O_3 (1385°C) was not reached. In order to establish conditions for maintaining melt saturated with oxygen the composition of initial charge was changed and an additional test CORD27 was conducted.

Table 5. Experimental procedure of CORD27 in air

Time from the test start, s	Stage/experimental activity
0-3200	Startup heating, molten pool formation; measurement of its depth (~ 40 mm), and bottom crust (~ 1.5 mm). Temperature of the molten pool surface ~ 1520ºC.
3200-4170	Electromagnetic screen is moved, liquidus temperature is measured by the VPA IMCC (Fig. 7, T_{liq} =1369ºC), melt sample is taken.
4170-4340	Melt exposition, crucible is moved downwards (~ 14 mm) until the generator reacts to the change of position (anode current changes).
4380-7840	The drive for the vertical movement of the crucible is turned on (at 9 mm/h).
7840-10200	The drive for the vertical movement of the crucible is turned off. The melt is exposed at ~ 1350-1370ºC for its saturation with oxygen. Uncontrolled gradual crystallization of the remaining liquid.
10204	HF heating is disconnected. Ingot is crystallized and cooled down. Temperature of the last liquid measured by pyrometer is ~1340ºC

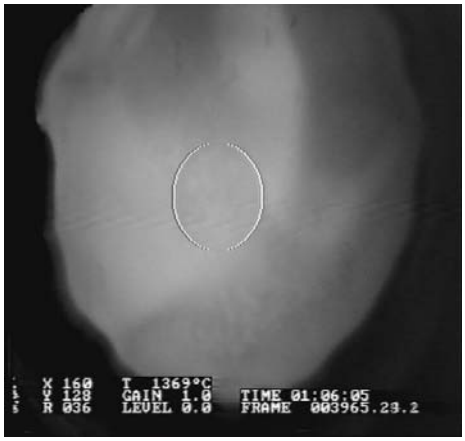

Fig. 7. Video image of the melt surface during the liquidus temperature measurements

Experiment CORD31 was aimed at specifying the eutectics composition. The initial charge composition was chosen using the results of SEM/EDX analysis of the eutectic zone from the CORD25 ingot .

Table 6. Experimental procedure of CORD31 in the inert atmosphere

Time from the test start, s	Stage/experimental activity
0-755	Startup heating, molten pool formation; measurement of its depth (~ 47 mm) and bottom crust (~ 5 mm). Temperature of the molten pool surface ~ 1520ºC..
755-2157	Electromagnetic screen is moved, liquidus temperature is measured by the VPA IMCC (Fig. 8, T_{liq} =1334ºC), melt sample is taken.
2157-2450	Melt exposition, crucible is moved downwards (~ 14 mm) until the generator reacts to the change of position (anode current changes)
2710-19800	The drive for the vertical movement of the crucible is turned on (at 9 mm/h).
19800	HF heating is disconnected. Ingot is crystallized in argon and cooled down. Temperature of the last liquid measured by pyrometer is ~ 1330ºC.

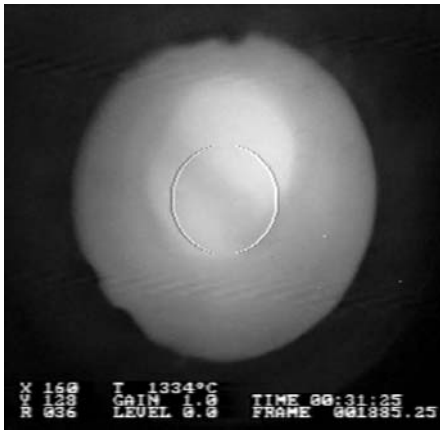

Fig. 8. Video image of the melt surface during the liquidus temperature measurements

A lower (in comparison with CORD25) liquidus temperature of the initial melt composition measured in this experiment indicates that the startup composition was closer to the ternary eutectics.

3. Posttest analysis

A set of physicochemical studies was completed in order to determine eutectics composition and temperature, to study the melt crystallization pattern and final solubility of components.

3.1. Chemical analysis

Melt samples from CORD-25-27, 31 and specimens cleaved from the crystallized ingots have been analyzed for the content of Fe^0, Fe^{2+}, Fe^{3+}, U^{4+} and U^{6+}.

The samples for analysis were handled in argon. They were crushed down to the grain size <50 μm.

The content of Fe^0 was determined by the copper-sulfate method.

The method is based on the displacement of copper by metallic iron, which takes place when corium powder is treated with copper sulfate [8,9]. Ions Fe^{2+}, which are equivalent to Fe_{met}, are titrated with $K_2Cr_2O_7$ solution in presence of the redox indicator: potassium difinylaminosupfonate ($C_6H_5NHC_6H_4SO_3Na$).

The method enables to determine the concentration of metallic iron in corium powder, when iron concentration is below 0.1 mass.%.

Fe(II) and Fe(III) content was determined by the method of photocolorimetry with orthophenanthroline ($C_{12}H_8N_2 \cdot H_2O$), which is applied for determining the content of iron oxides in the samples of uranium-bearing corium without uranium separation [10]. The range of measured iron concentrations is 0.4-400 mg/dm^3. The total relative error of the method does not exceed ±3%, if the measured optical densities are within 0.2-0.6.

The method is based on the reaction between orthophenanthroline and ions of ferrous iron in the pH 3-9 range, at which an orange-red complex is formed. The coloring intensifies quickly at pH 3.0-3.5 in presence of excessive phenanthroline and it remains stable during several days. The mass concentration of total iron is determined by reducing iron (III) to iron (II) by hydroxylamine in the acid conditions; iron (II) is measured directly. The content of ferric iron is calculated from the difference between the content of iron (II) and total iron [11,12].

The methodology of determining U^{+4}, U^{+6} using arsenazo III reagent ($C_{22}H_{18}O_{14}N_4S_2As_2Na_2$) is applied for identifying microquantities of uranium in corium samples without its separation, its sensitivity is 0.04 μg/ml [16, 17].

The methodology of determining U^{+4}, U^{+6} using arsenazo III reagent is applied for identifying microquantities of uranium in corium samples without its separation, its sensitivity is 0.04 μg/ml [17,18].

The method enables to determine the content of quadrivalent uranium and total uranium in the solution separately. The reduction of hexavalent to quadrivalent uranium is performed in 4 N HCl using the granulated metallic zinc. The amount of U (VI) is calculated from the difference between U (IV) and total U.

The results of Fe^0, Fe^{2+}, Fe^{3+}, U^{4+} and U^{6+} determination are presented in Table 7.

Table 8 gives the compositions of samples CORD-25-27, which were calculated from the results of chemical analysis.

Table 7. Results of chemical analysis of samples from CORD-25-27, 31

CORD	Sample	Fe^0	Fe^{2+}	Fe^{3+}	U^{4+}	U^{+6}
		mass%				
25 (Ar)	Melt	3.4	56.4	6.0	7.0	not found
26 (Air)	Melt	0	16.9	23.5	27.7	not found
27 (Air)	Ingot top	not determined	11.6	9.8	30.2	28.2
	Melt	0	15.6	8.5	41.1	11.5
31 (Ar)	Ingot top	0.3	44.7	6.2	13.5	not found.

[1)] – Sample cleaved from the eutectic part of the ingot.

Table 8. Composition of samples from CORD-25-27, 31

CORD	Sample	FeO_y		UO_x	
		y	Content, mass%/mole%		x
25 (Ar)	Melt	1.04	85.4/92.0	7.9/2.3	2.00
26 (Air)	Melt	1.31	55.6/67.1	31.4/14.8	2.00
27 (Air)	Melt	1.21	32.4/55.0	60.2/32.9	2.22
	Ingot top	1.26	29.1/52.0	67.5/41.7	2.48
31 (Ar)	Ingot top	1.10	70.9/82.2	15.3/4.9	2.00

In the samples of experiments made in the inert atmosphere the metallic iron was found, which indicates that iron oxide became stoichiometric as $Fe_{0.95}O$.

In the samples of experiments made in air (e.g., CORD27) the melt saturation with oxygen during its exposition was observed.

Table 9 shows errors of the chemical analyses.

Table 9. Relative errors of chemical analyses

Element	Method	Error, % rel.
Fe^{+2}, Fe^{+3}, U^{+4}, U^{+6}	Photocolorimetry	5
Fe^0	Copper-sulfate	10

3.2. Material balance of tests

In order to determine the material balance of tests the initial charge components and molten products were weighed with 0.1 g accuracy.

Table 10 gives the data on material balance of CORD25-27, 31.

Table 10. Material balance of CORD 25-27, 31

CORD	Introduced, g		Collected, g	
25	UO_2	19.6	Ingot	262.4
	ZrO_2	8.4	Melt sample	10.5
	Fe	28.6	From the probe	3.2
	FeO	230.6	Dry spillages	10.1
	Σ	**287.2**	Σ	**286.2**
	Imbalance	**1.0**		
26 (in air)	UO_2	67.5	Ingot	193.8
	ZrO_2	7.5	Melt sample	11.7
	Fe	5.0	Accretions	64.7
	Fe_2O_3	220.0	From the probe	16.2
			Dry spillages	15.2
	Σ	**300.0**	Σ	**301.6**
	Imbalance	**+1.6**		
27 (in air)	$UO_{2.24}$	194.7	Ingot	303.9
	ZrO_2	6.5	Melt sample	2.8
	Fe	8.1	Dry spillages	12.7
	Fe_2O_3	123.3	Accretions	16.1
	Σ	**332.6**	Σ	**335.5**
	Imbalance	**+2.9**		
31	UO_2	64.2	Ingot	295.0
	ZrO_2	20.7	Melt sample	1.2
	FeO	196.7	From the probe	1.4
	Fe	23.1	Dry spillages	6.1
	Σ	**304.7**	Σ	**303.7**
	Imbalance	**1.0**		

The weight of crystallized ingots and insignificant imbalance of the experiments (except CORD26) indicates the complete melting of introduced substances and proves the adequacy of completed studies. The posttest analysis of CORD26 ingot was not made.

3.3. SEM/EDX analysis

The determination of ingot microstructure and elemental composition was performed by the scanning electron microscopy (SEM) and energy-dispersion X-ray analysis (EDX).

The examination of specimens by SEM was made using the scanning electron microscope ABT-55. The elemental composition of chosen specimen sections was performed using 'Oxford Link' micro-probe .

The spectral characteristics of each specimen were determined. The characteristics were used for identifying the specimen integral composition and the composition of each separate phase. The quantitative analysis was performed by comparing spectrum intensities of the reference substance (extra pure, specially prepared) and studied specimen. The used reference specimens of U, Zr, Cr, Fe, Si, Ca, Ni were taken from the «Link" reference kit.

The reliable identification limit of an element depends on its number in the Mendeleyev periodical table; it varies between 0.3 mass.% to 0.5 mass.%. The detection of elements in smaller quantities is unreliable.

EDX-analyzer using microscope ABT-55 is not sensitive to light elements (to oxygen, in particular). For this reason oxygen was determined from the mass deficit; the oxygen determination error was ~5 mass.%.

Posttest ingots were cut along the axis, their halves and quarters were used for preparing sections for analysis. By the microscope scanning of the specimens the ternary eutectics zone was found and the analysis of its coexisting phases was performed.

As during CORD26 the melt was not maintained at the temperature corresponding to the oxidation of Fe_3O_4 to Fe_2O_3, the test ingot was not used for analysis.

CORD25

Fig. 9 presents the CORD25 section with marked locations of SEM/EDX. The ternary eutectics zone was found in locations 8 and 9. Figs. 10-14 show the microphotographs of locations 1 - 10.

The excess of metallic iron crystallized on the pool bottom in the form of thin layers alternated with FeO, which were directed at a right angle to the crystal growth front (location10, point P1 in Fig. 14), and in the eutectic zone as separate rounded inclusions (Fig. 12, point P4).

The crystallization pattern of the eutectic zone and adjacent regions proves that the refractory phase of FeO was the first to precipitate (Fig. 12 point P2). It was followed by the secondary crystallization of FeO and solid solution $UO_2(ZrO_2,FeO)$ (Fig. 12, point P3). After that the crystallization of ternary eutectics started (Fig. 12, area SQ2).

It is known from the published data and our investigations that UO_2 and ZrO_2 form limited solid solutions in the subsolidus domain; and FeO partially dissolves in each of them. Consequently, in the subsolidus domain of the ternary system the appearance of FeO and solid solutions $UO_2(ZrO_2,FeO)$ and $ZrO_2(UO_2,FeO)$ can be expected.

The crystals of solid solutions, which are formed in the subsolidus region near the eutectics, have small sizes (Fig 12, points P1 and P3), for this reason their analysis gives a considerable excess of FeO content. But in location 9, which corresponds to a slow melt cooling (Fig. 13, point P1), the crystals of solid solutions grew to the size sufficient for the EDX analysis avoiding the considerable influence of FeO phase surrounding them.

It follows from the SEM/EDX analysis that the solubility of FeO in the $U(Zr)O_2$-based solid solution in the subsolidus domain is ~10 mole% (3 mass %) (Fig. 13, point P1). At the same time the solubility of FeO in the solid solution $Zr(U)O_2$ was not observed due to the small size of crystallized phase (Fig. 13, point P2).

The approximate composition of ternary eutectics corresponds to ~7 mole% UO_2, 5 mole% ZrO_2 and 88 mole% FeO (21.4 mass.% UO_2, 6.9 mass.% ZrO_2 and 71.7 mass.% FeO), which has a good agreement with predicted position of the ternary eutectics zone (see. Fig. 12, location SQ2). In spite of that, the crystallized ternary eutectic zone was not large enough for reliable analysis.

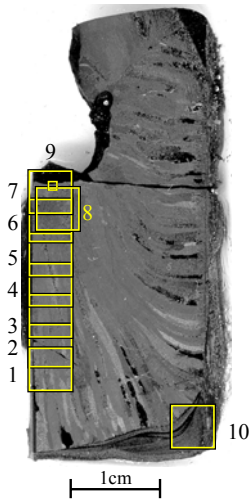

Fig. 9. CORD25 template with marked locations of studies

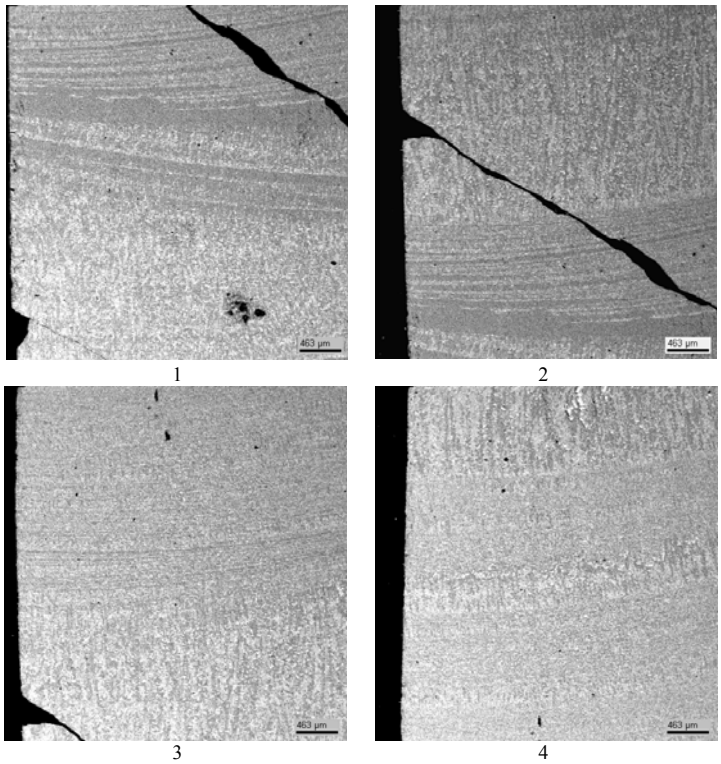

Fig. 10. Microphotographs of locations 1, 2, 3 and 4 of CORD25 ingot

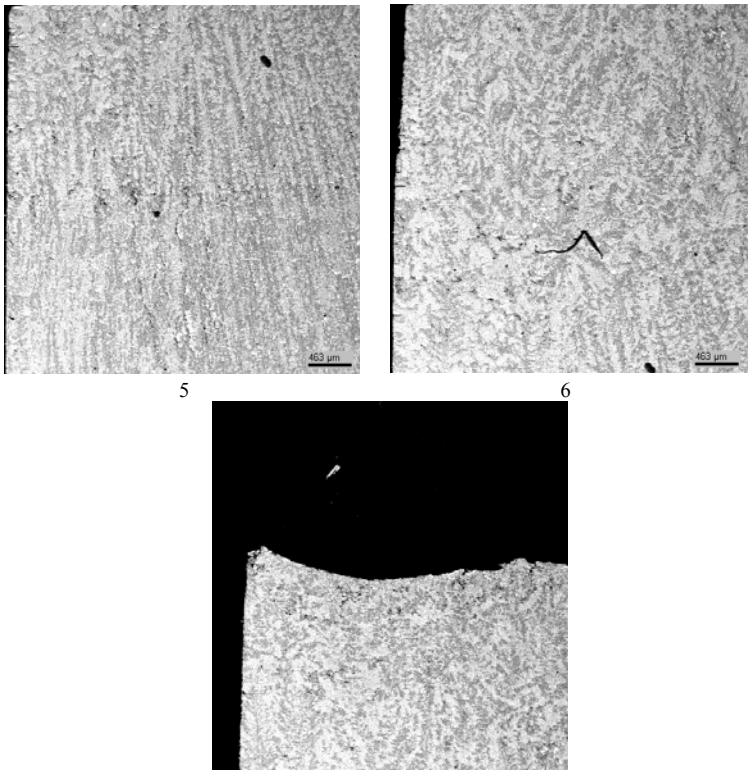

Fig. 11. Microphotographs of locations 5, 6 and 7 of CORD25 ingot

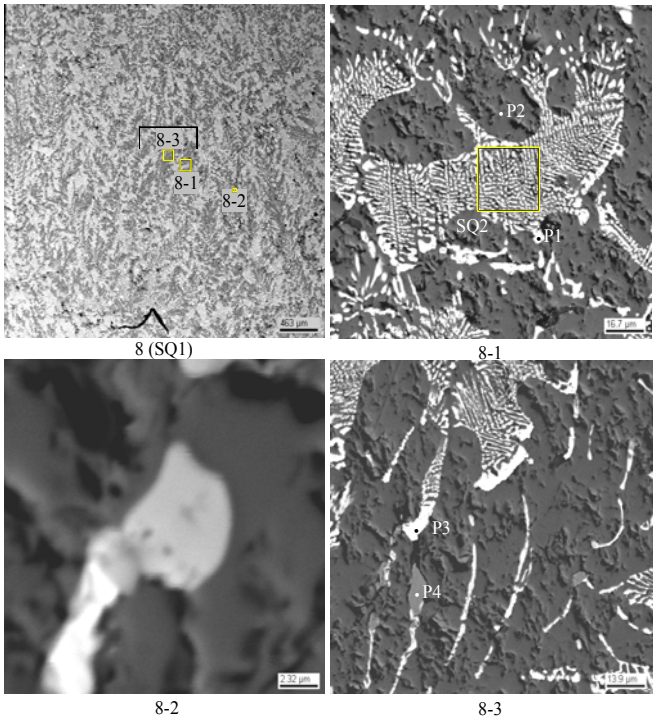

№		UO_2	ZrO_2	FeO
SQ1	mass%	11.81	6.2	81.99
	mole%	3.54	4.07	92.39
SQ2	mass%	21.38	6.89	71.73
	mole%	6.98	4.93	88.08
P1	mass%	49.08	12.94	37.98
	mole%	22.29	12.88	64.83
P2	mass%	-	0.68	99.32
	mole%	-	0.4	99.6
P3	mass%	84.58	9.65	5.77
	mole%	66.37	16.60	17.03

№		U	Zr	Fe
P4	mass%	0.95	3.15	95.90
	mole%	0.23	1.97	97.81

Fig. 12. Microphotograph of location 8 (ternary eutectics) of CORD25 ingot. EDX-analysis data

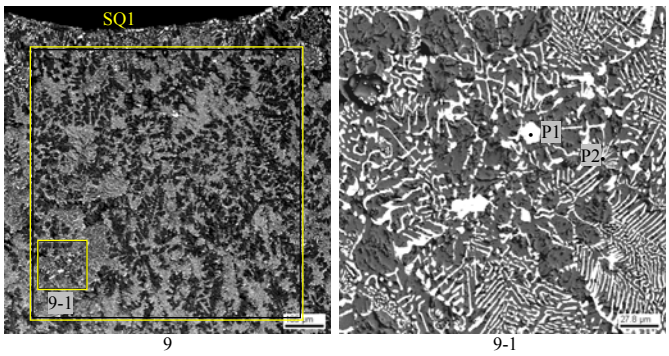

№		UO_2	ZrO_2	FeO
SQ1	mass%	12.07	5.69	82.24
	mole%	3.62	3.74	92.65
P1	mass%	92.08	4.86	3.06
	mole%	80.62	9.33	10.05
P2	mass%	29.71	47.14	23.15
	mole%	13.50	46.95	39.55

Fig. 13. Microphotograph of location 9 (ternary eutectics) of CORD25. EDX-analysis data

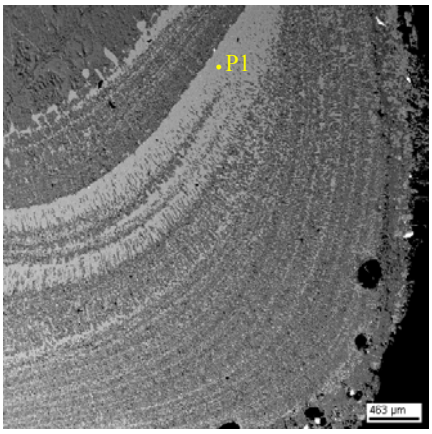

№		Fe
P1	mass%	100
	mole%	100

Fig. 14. Microphotograph of location 10 of CORD25 ingot. EDX-analysis data

CORD27

The composition of initial charge was prepared to be close to the calculated eutectics, which is evident in the ingot crystallization pattern. Fig. 15 shows the ingot section from CORD27 with marked locations taken for analysis.

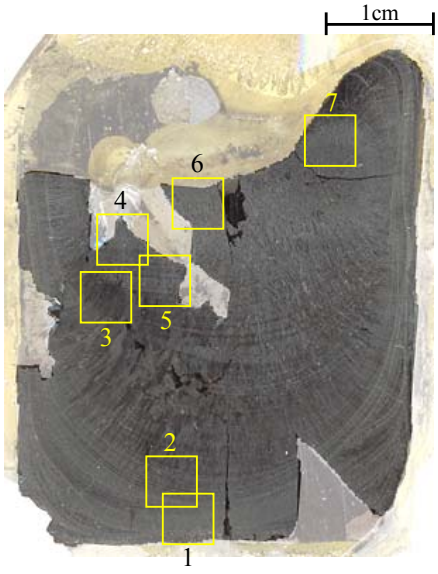

Fig. 15. CORD27 template with studied locations

Figs. 16-22 show the microphotographs of marked locations and results of EDX analysis.

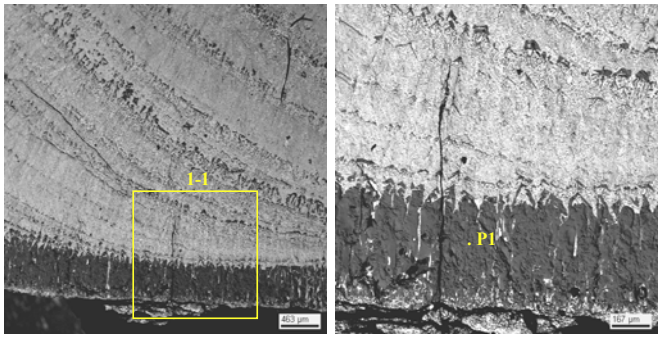

1 1-1(SQ1)

№		U	Zr	Fe	O
SQ1	mass%	45.67	-	27.10	27.23
	mole%	8.06	-	20.40	71.54
P1	mass%	-	-	60.51	39.49
	mole%	-	-	30.51	69.49

Fig. 16. Microphotograph of location 1 of CORD27 template. EDX-analysis data

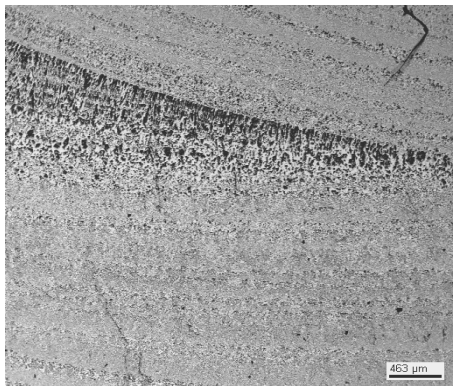

2

Fig. 17. Microphotograph of location 2 of CORD27 template

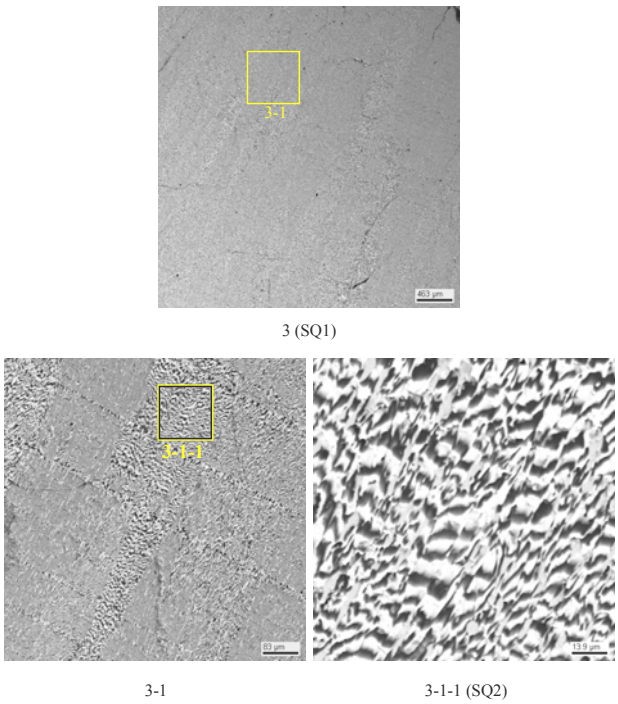

№		U	Zr	Fe	O
SQ1	mass%	44.65	1.34	23.57	30.44
	mole%	7.42	0.58	16.70	75.29
SQ2	mass%	47.97	1.27	24.99	25.78
	mole%	8.86	0.61	19.68	70.85

Fig. 18. Microphotographs of location 3 of CORD27 template. EDX-analysis data

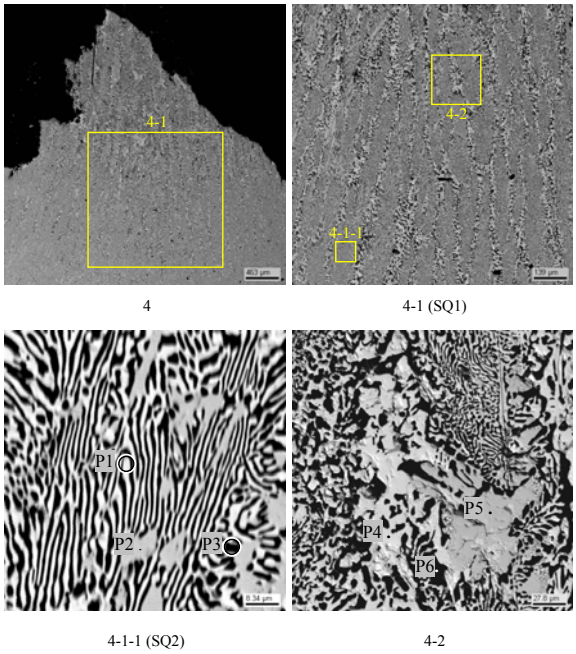

№		U	Zr	Fe	O
SQ1	mass%	46.38	1.25	24.01	28.37
	mole%	8.08	0.57	17.83	73.53
SQ2	mass%	46.48	1.30	24.33	27.89
	mole%	8.18	0.60	18.24	72.98
P1	mass%	24.01	1.09	48.01	26.89
	mole%	3.80	0.45	32.40	63.35
P2	mass%	58.63	5.38	11.58	24.42
	mole%	12.08	2.89	10.17	74.86
P3	mass%	13.61	1.43	52.92	32.04
	mole%	1.89	0.52	31.34	66.25
P4	mass%	72.17	0.32	0.56	26.96
	mole%	15.15	0.18	0.50	84.18
P5	mass%	60.73	3.11	11.21	24.95
	mole%	12.45	1.66	9.79	76.09
P6	mass%	1.53	0.62	58.04	39.37
	mole%	0.18	0.19	29.56	69.99

Fig. 19. Microphotographs of location 4 of CORD27 template. EDX-analysis data

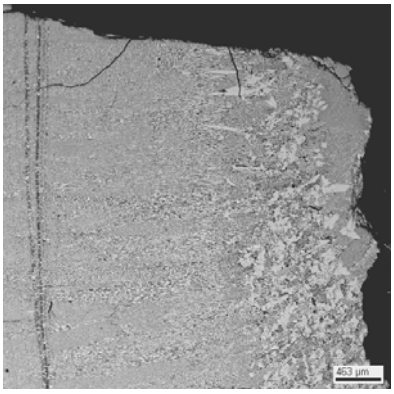

5

Fig. 20. Microphotographs of location 5 of CORD27 template

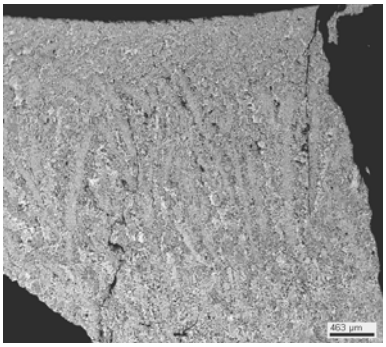

6 (SQ1)

№		U	Zr	Fe	O
SQ1	mass%	42.60	1.04	23.89	31.44
	mole%	6.90	0.44	16.50	75.78

Fig. 21. Microphotographs of location 6 of CORD27 template. EDX-analysis data

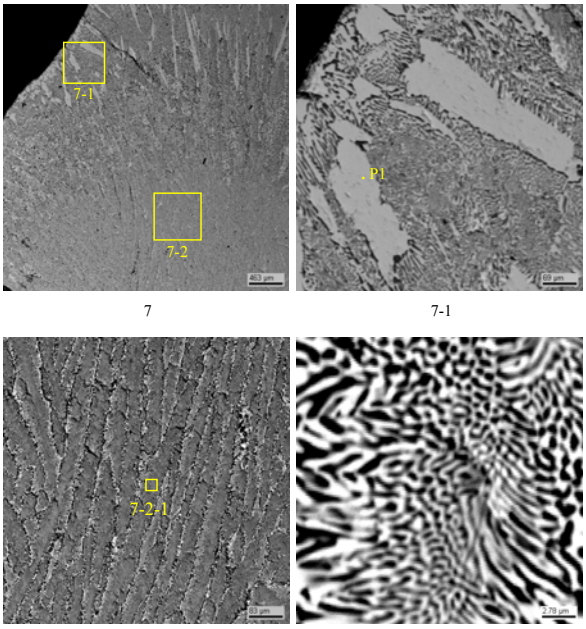

7 7-1

7-2 (SQ1) 7-2-1 (SQ2)

№		U	Zr	Fe	O
SQ1	mass%	49.17	1.09	24.47	25.26
	mole%	9.24	0.54	19.6	70.62
SQ2	mass%	50.49	1.23	24.55	23.83
	mole%	9.85	0.63	20.33	69.19
P1	mass%	60.57	3.74	11.32	24.37
	mole%	12.59	2.03	10.03	75.35

Fig. 22. Microphotographs of location 7 of CORD27 template. EDX-analysis data

The microstructural pattern of locations 3-7 proves the eutectic character of their crystallization. It is also confirmed by the similarity of average compositions (Fig. 18, segments SQ1, SQ2; Fig. 19, segments SQ1, SQ2; Fig. 22, segments SQ1, SQ2).

The EDX analysis shows that the discussed microstructure includes three phases: grey, white and black (from the contrast of images on electronic microphotographs).

The grey phase analyzed in point P5 (Fig. 19) and in point P1 (Fig. 22) has a high content of uranium, iron and oxygen, and a small amount of Zr. This composition enables to assume the formation of solid solution based on the $UFeO_4$ compound, which was previously detected in [18,19]. Solid solution $U(Zr)FeO_4$ is observed as grains having the typical size of 30-50 μm in the non-eutectic crystallization domain (Fig 19, location 4-2, point P5; Fig. 22, location 7-1, point P1) and as finer grains – below 10 μm, in the eutectic crystallization domain (Fig 19, location 4-1-1, point P2).

The white phase is a solid solution of Zr and Fe oxides based on U oxides (Fig. 19, point P4). The final solubility of iron oxide in the solid solution of $UO_{2+x}(ZrO_2,FeO_y)$ in the subsolidus region is evaluated as 3.2 mole % (recalculated to $FeO_{1.5}$. Fig. 19, point P4).

The black phase is iron oxide (Fig. 19, points P6).

X-ray fluorescence (XRF) was used for the structural identification of phases. A sample from location 7 (Fig. 15) was taken for analysis. The XRF showed the presence of four, not three phases: 1) α-Fe_2O_3- based, 2) U_3O_8-based (probably solid solution $U_3O_8(ZrO_2,Fe_2O_3)$); 3) U_3O_7-based (probably solid solution $U_3O_7(ZrO_2,Fe_2O_3)$) and 4) $UFeO_4$-based (probably solid solution $U(Zr)FeO_4$) (Fig. 23). In spite of the overlapping of main reflexes and reflexes of U_3O_8-based phase, the last phase was identified from the reflexes on the corners of 46 and 62 (Fig. 23).

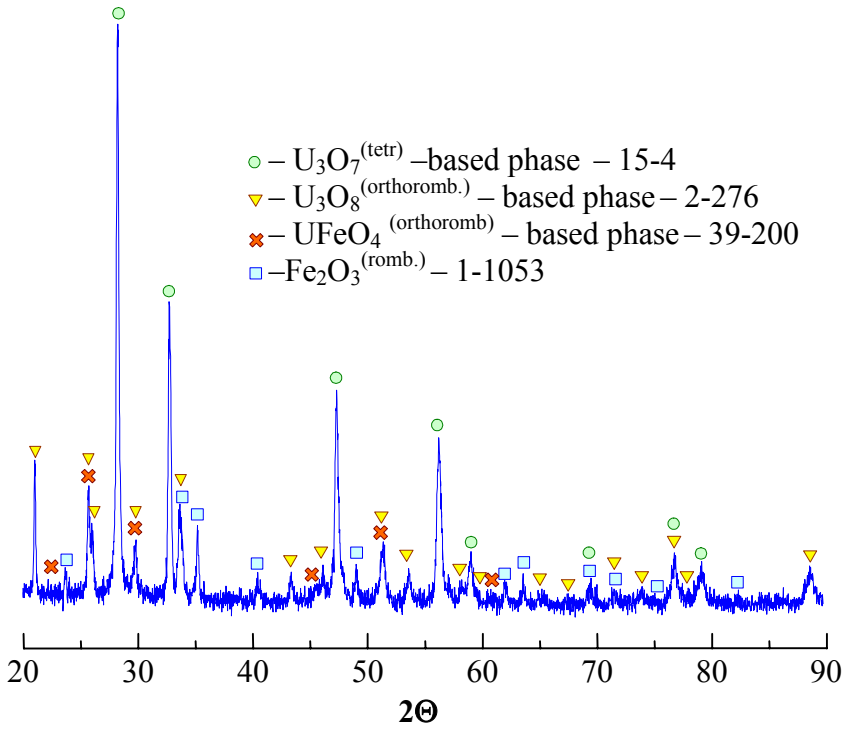

Fig. 23. Difractogram of a sample from the eutectic region of the ingot (Cu_{K_α}-radiation)

The formation of a large quantity of U_3O_7-based solid solution, which is a low-temperature and less than U_3O_8 oxygen-saturated phase (Fig. 23), is likely to be caused by the decomposition of an O- and Fe-deficient U(Zr)FeO_4-based solid solution in a solid phase into Fe_2O_3 and solid solution based on U_3O_7. This assumption explains both a high content of U_3O_7-based phase and a relatively small (taking into account the position of the studied composition in the concentration triangle Fe_2O_3-$UFeO_4$-UO_2) content of $UFeO_4$. This is confirmed by SEM-images of the $UFeO_4$-based solid solution (Fig. 19, location 4-2). The black and white fractions visible on the grain borders and inside them can be explained as the results of its decomposition.

We should note the absence of ZrO_2 in the lower template zone (Fig. 15, location 1), which is explained by the experimental procedure: the molten pool of $UO_{2.24}$ and Fe_2O_3 (Fig. 16, segment SQ1) was established in the beginning of melting, after that ZrO_2 was introduced.

CORD31

Fig. 24 shows the ingot section from test CORD31, in which the examined locations are marked. Figs. 25-33 present the microphotographs of the marked locations.

It should be noted that, differently from CORD25, a UO_2-based refractory phase of solid solution starts to crystallize on the molten pool bottom (Fig. 27, location 3). It means that the figurative point of the composition is in the domain of the primary crystallization of UO_2-based solid solution. All other studied locations of the template had a eutectic structure, which indicates that the composition was close to the ternary eutectics. Most extensive zones of the ternary eutectics crystallization were found in locations 1 and 5 (Fig. 24), in the part of the ingot shrink cavity. Barely detectable phase contrast of coexisting solid solutions based on UO_2 and on ZrO_2 made their identification complicated.

Just like in case of CORD25, the solubility of FeO in both types of solid solutions was found. First of them is UO_2(ZrO_2,FeO)- based (Fig. 28, points P1, P2, P3), second – ZrO_2(UO_2,FeO)-based (Fig. 25, points P5 and P6). The solubility limit of the first solid solution is 8±2 mole% FeO. Due to the small size of grains the solubility limit of the second solution can hardly be determined directly, but it can be evaluated as ~20 mole% FeO. Due to the peculiarities of a solid solution crystallization in the UO_2-FeO system it can be assumed that the solubility limit of a UO_2-based solid solution can be considerably higher due to its decomposition into U(Zr)O_2 and FeO.

The specified composition of ternary eutectics is 3.6 mole% UO_2, 4.9 mole% ZrO_2 and 91.5 mole% FeO (11.8 mass% UO_2, 7.4 mass% ZrO_2 and 80.8 mass% FeO) (Fig. 28, region SQ1), which has a good agreement with a predicted position of the ternary eutectic zone (Fig. 3).

The data provided by the studies of ternary eutectic zone of the CORD-25 ingot give a slightly higher UO_2 concentration in comparison with CORD-31 data. It is explained by the following: large crystals of the UO_2(ZrO_2,FeO)-based solid solution were included into the analysis of CORD-25 ternary eutectic zone (Fig. 12, location 8-1, segment SQ2).

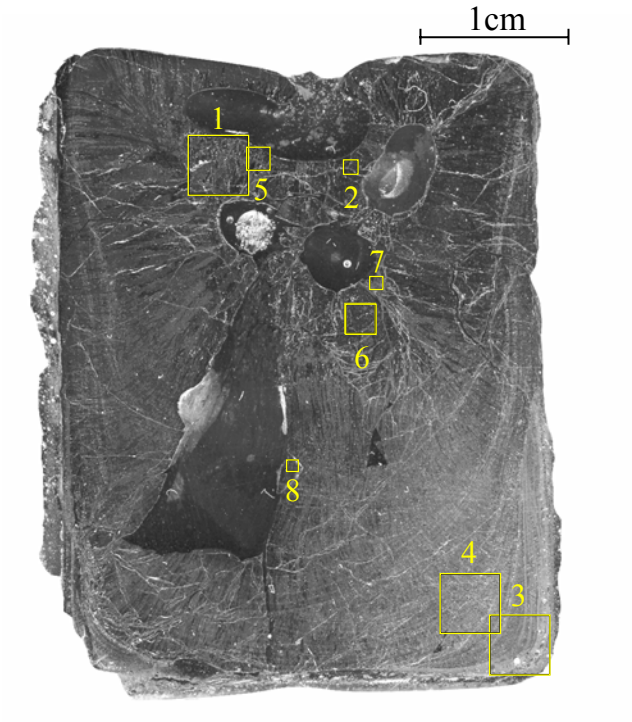

Fig. 24. CORD31 template with studied locations

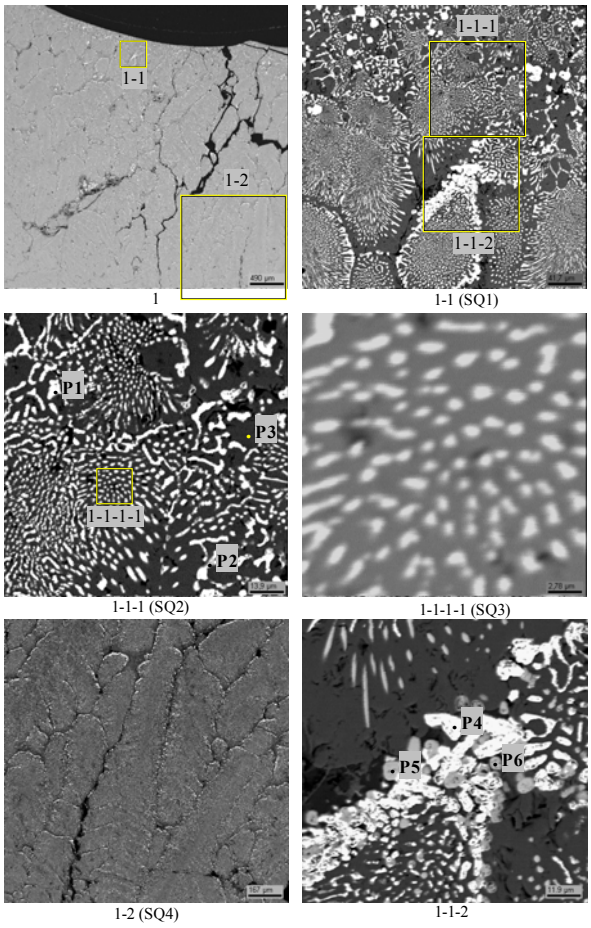

№		UO_2	ZrO_2	FeO
SQ1	mass%	13.04	7.22	79.74
	mole%	3.97	4.82	91.22
SQ2	mass%	11.57	7.04	81.4
	mole%	3.47	4.63	91.89
SQ3	mass%	10.61	8.1	81.29
	mole%	3.18	5.32	91.51
SQ4	mass%	13.00	6.50	80.50
	mole%	3.94	4.32	91.74
P1	mass%	49.89	6.04	44.07
	mole%	21.81	5.79	72.4
P2	mass%	21.6	29.67	48.73
	mole%	8.01	24.1	67.89
P3	mass%	-	-	100
	mole%	-	-	100
P4	mass%	91.09	5.32	3.58
	mole%	78.37	10.04	11.59
P5	mass%	40.25	49.71	10.04
	mole%	21.53	58.27	20.19
P6	mass%	38.10	50.70	11.20
	mole%	19.92	58.08	22.00

Fig. 25. Microphotograph of location 1, CORD31 template. EDX-analysis data

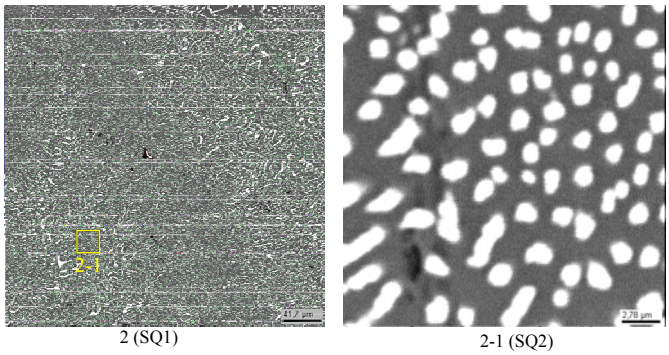

2 (SQ1) 2-1 (SQ2)

№		UO_2	ZrO_2	FeO
SQ1	mass%	12.36	7.21	80.43
	mole%	3.74	4.78	91.48
SQ2	mass%	8.1	8.51	83.4
	mole%	2.38	5.48	92.14

Fig. 26. Microphotograph of location 2 of CORD31 template. EDX-analysis data

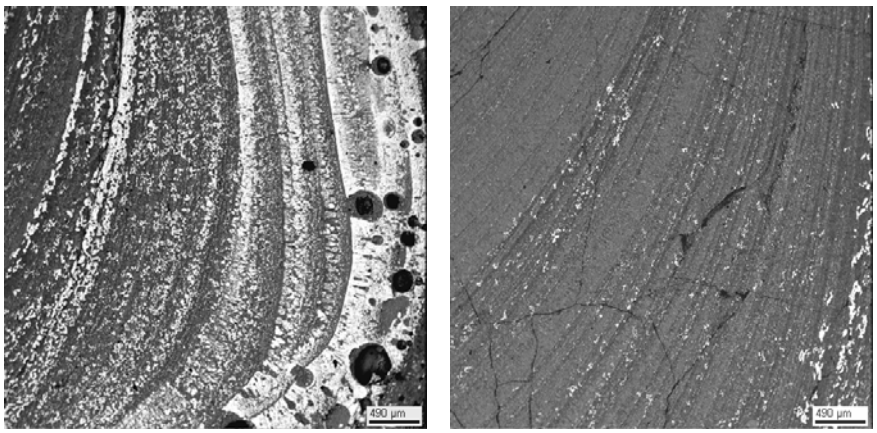

3 4

Fig. 27. Microphotographs of locations 3 and 4 of CORD31 template

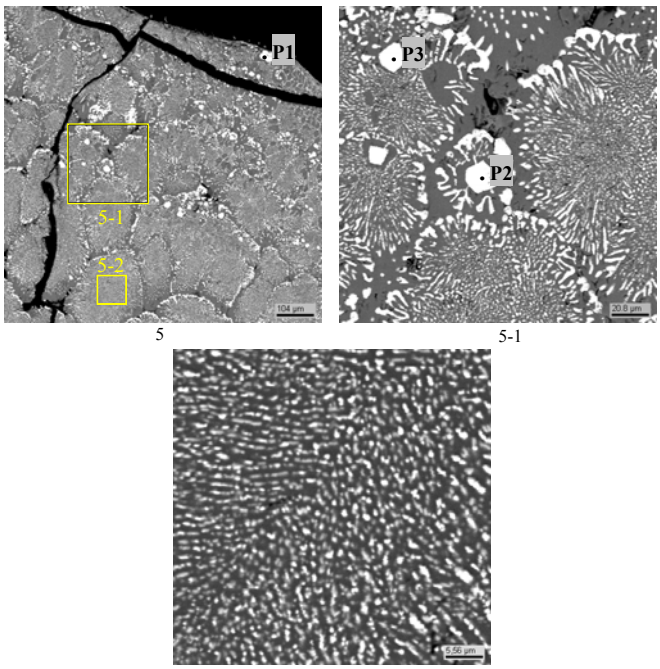

5 5-1

5-2 (SQ1)

№		UO_2	ZrO_2	FeO
SQ1	mass%	11.79	7.38	80.83
	mole%	3.55	4.88	91.57
P1	mass%	87.82	10.11	2.07
	mole%	74.58	18.82	6.61
P2	mass%	90.69	6.77	2.54
	mole%	78.81	12.89	8.30
P3	mass%	88.65	7.82	3.53
	mole%	74.47	14.40	11.14

Fig. 28. Microphotograph of location 5, CORD31 template. EDX-analysis data

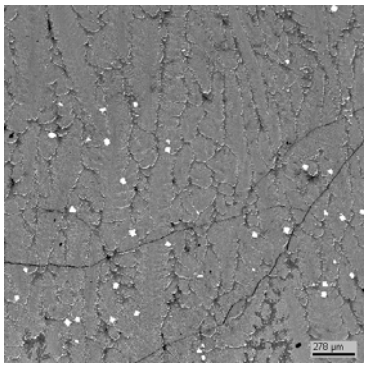

6 (SQ1)

№		UO_2	ZrO_2	FeO
SQ1	mass%	13.85	6.55	79.60
	mole%	4.23	4.38	91.39

Fig. 29. Microphotograph of location 6, CORD31 template. EDX-analysis data

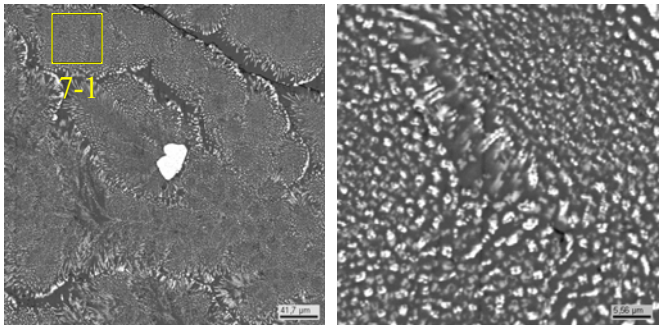

7 7-1 (SQ1)

№		UO_2	ZrO_2	FeO
SQ1	mass%	15.19	7.27	77.54
	mole%	4.71	4.94	90.35

Fig. 30. Microphotograph of location 7, CORD31 template. EDX-analysis data

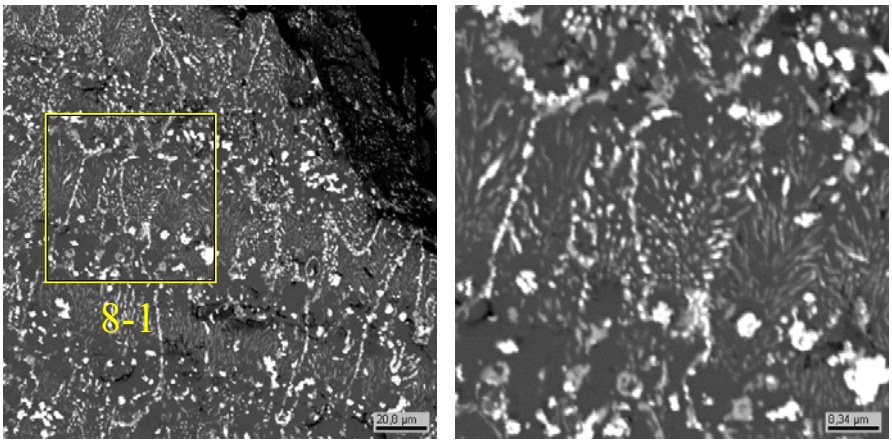

8 8-1

Fig. 31. Microphotograph of location 8, CORD31 template

3.4. Differential thermal analysis

The powder specimens prepared from the ternary eutectics crystallization zones were studied using the SETSYS Evolution-2400 analyzer (Fig. 32), which enables to get information about the behavior of substances in a wide range of temperatures – from 196 to 2400°C. The error in determining the temperature of phase transitions was ±5°C.

The gas-tight experimental section can be used for getting DSC, DTA, TG-DSC and TG-DTA curves in vacuum and different atmospheres (air, argon, helium, CO_2), which is necessary for studying systems containing elements, the oxidation degree of which depends on the oxygen partial pressure.

The SETSOFT software operates the device and enables to collect and process data.

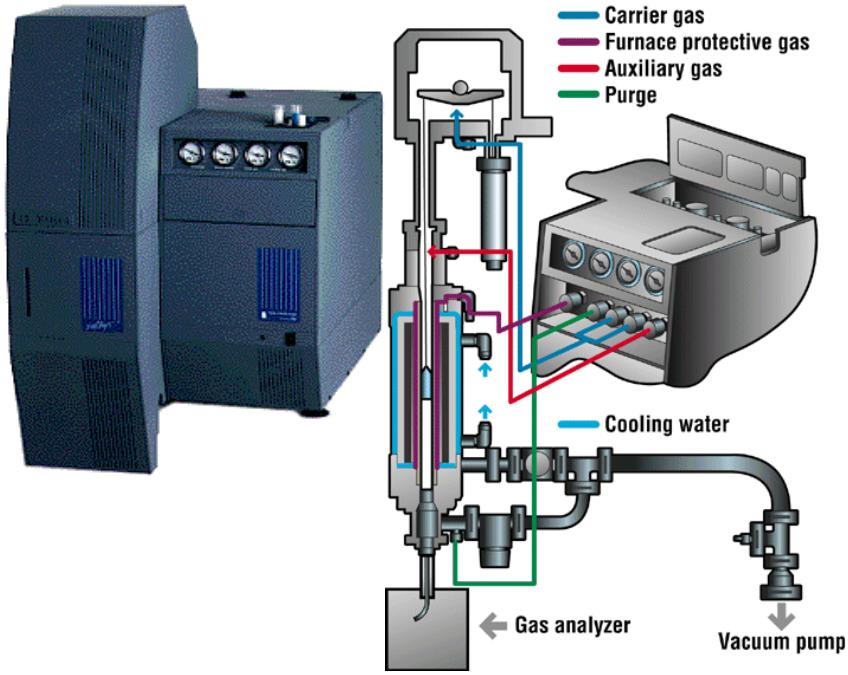

Fig. 32. Schematics of SETSYS Evolution-2400 thermoanalyzer

Solidus temperature (in our case the temperature of ternary eutectics) was determined from the beginning of endothermic effect at the specimen heating and the beginning of exothermic effect at its cooling. The different values of solidus temperature at heating and cooling are explained by a possible interaction of the specimen with crucible material, therefore the value measured at the specimen heating is considered as more reliable.

CORD25

Figs. 33-35 show the DTA curves of the CORD25 specimen. A sample for analysis was taken from location 7 (Fig. 9, 11).

The analysis parameters: sample mass ≈ 9mg; carrier gas – helium; carrier gas flow rate – 4ml/min.; thermocouple type – B (Pt-30%Rh vs. Pt - 6% Rh); heating rate–5°C/min. Crucible material –Al_2O_3.

Two distinct endothermic effects are observed in Fig. 33 in the temperature ranges 1321–1334°C and 1366–1393°C. The first corresponds to the solidus of a ternary system, in this case – ternary eutectics, the second – to the liquidus of the specimen with a given composition. The presence of two effects indicates that the specimen composition did not exactly correspond to the composition of ternary eutectics of UO_2-ZrO_2-FeO.

In order to determine the temperature, at which the effects start, the base line was chosen "linear from first to last point", after that tangents to the peak sides were plotted. The intersection of a tangent with the baseline provided 1321°C (T_{sol}) in the first case, and the second peak on the heating line corresponded to the liquidus temperature 1393°C (T_{liq}).

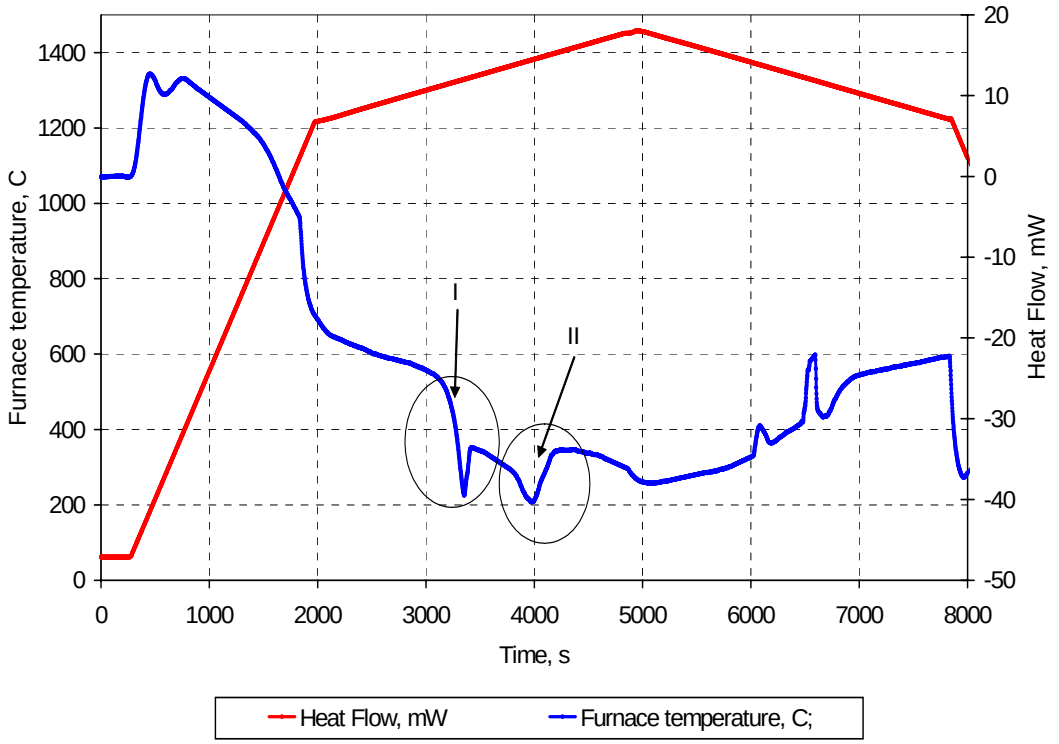

Fig. 33. Thermogram of CORD25 sample

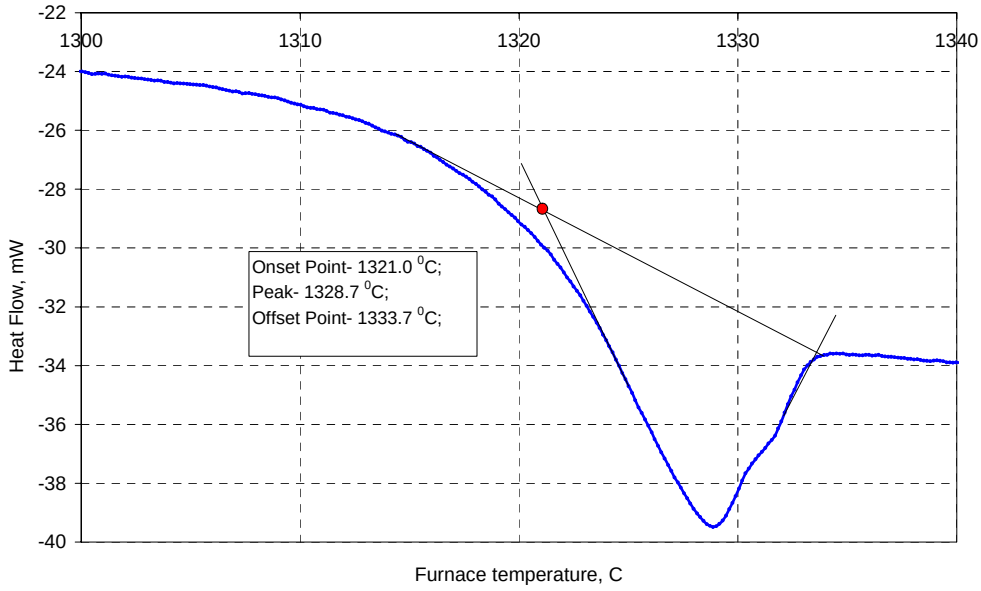

Fig. 34. Thermogram of CORD 25 sample – enlarged fragment I (at heating)

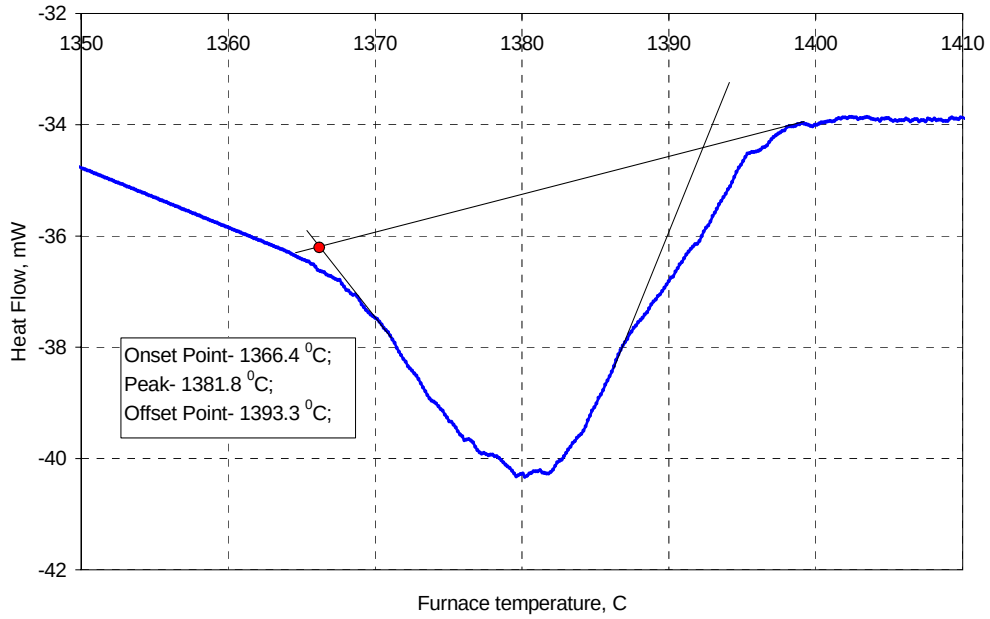

Fig. 35. Thermogram of CORD 25 sample – enlarged fragment II (at heating)

CORD27

Figs. 36 and 37 show the DTA curves of the CORD27 specimen. A sample for analysis was taken from location 6 (Fig. 15, 21).

The analysis parameters: sample mass ≈10 mg; carrier gas – air; thermocouple type – B (Pt-30%Rh vs. Pt - 6% Rh); heating rate –5°C/min. Crucible material –Al_2O_3.

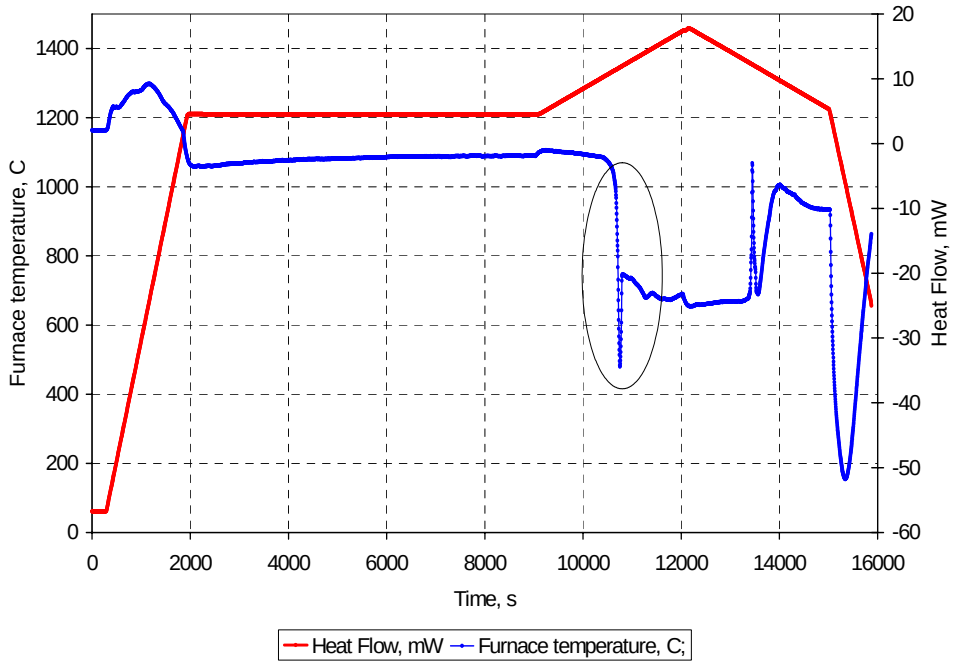

Fig. 36. Thermogram of CORD27 sample

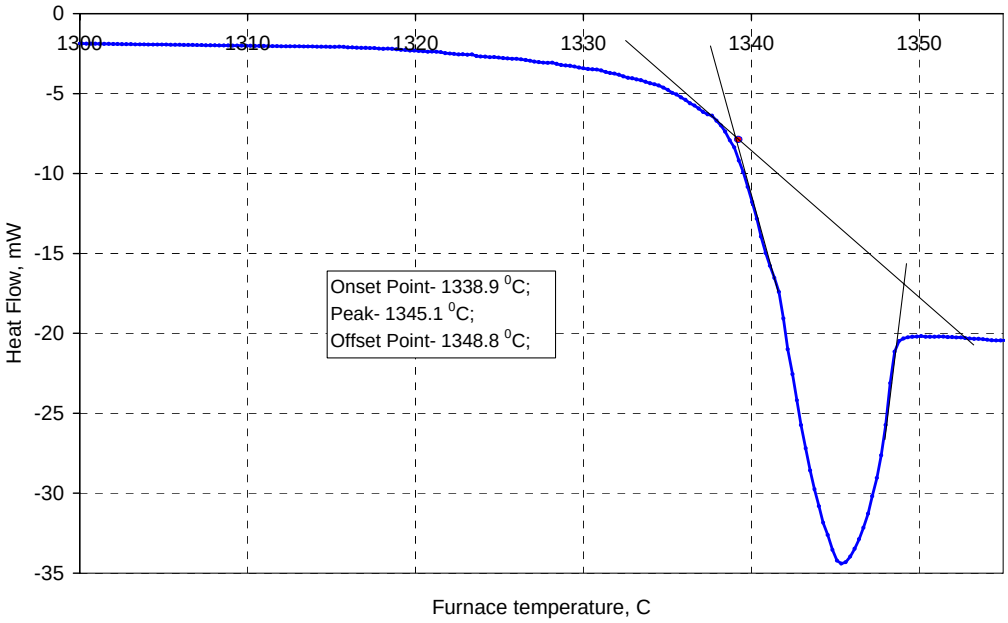

Fig. 37. Thermogram of CORD 27 sample – enlarged fragment I (at heating)

The presence of a single endothermic effect in the thermogram of CORD27 specimen (Fig. 36) means that the specimen corresponded to the eutectic composition of the UO_{2+x}-ZrO_2-FeO_y system for air.

The temperature of the ternary eutectic 1339°C was determined from the crossing of a tangent line plotted to the effect side slope with the baseline "linear from first to last point".

CORD-31

Figs. 38 and 39 show the DTA curves of the CORD31 specimen.

The analysis parameters: sample mass ≈7 mg; carrier gas – helium; carrier gas flow rate – 4 ml/min; heating rate -5 °C/min; thermocouple type - B (Pt-30%Rh vs. Pt - 6% Rh). Crucible material –Al_2O_3.

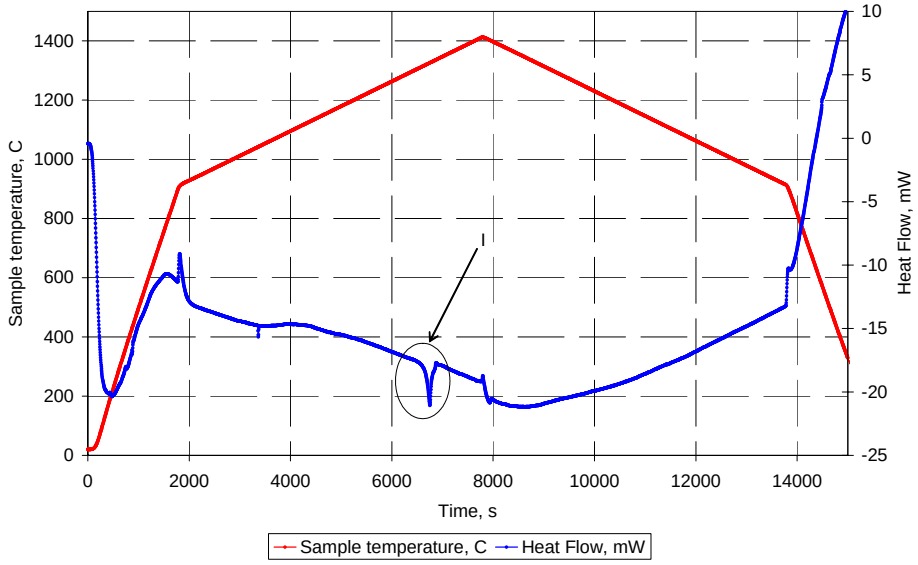

Fig. 38. Thermogram of CORD-31 sample

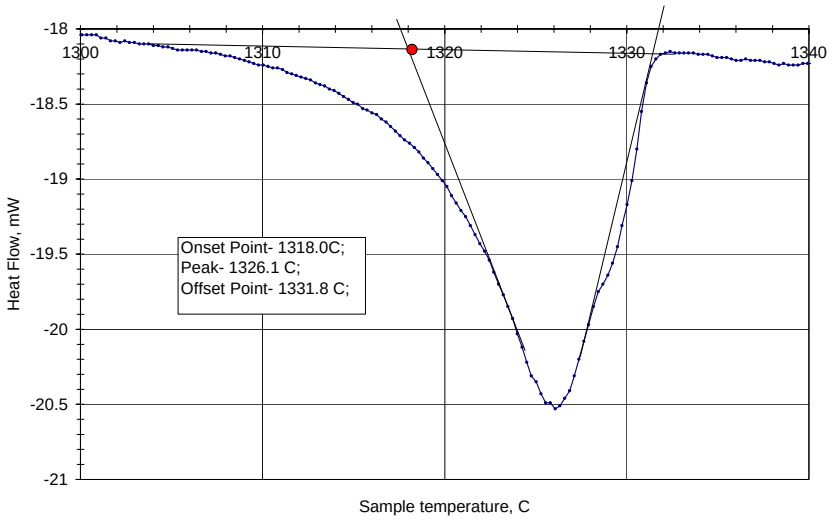

Fig. 39. Thermogram of CORD 31 sample – enlarged fragment I (at heating)

SEM/EDX analysis of the CORD-31 ingot did not show regions, which had compositions considerably different from eutectics. It should be noted that the specimen heating peak comprises two overlapping endothermic effects, the second of which is likely to be liquidus.

The solidus temperature of 1318°C was determined from the crossing of a tangent line to the effect slope with the baseline.

4. Discussion of results

Experiments conducted in the inert atmosphere (CORD-25, CORD-31) enabled to determine the composition and temperature of ternary eutectics in the UO_2-ZrO_2-FeO system, as well as the composition of crystallized phases. The data are summarized in Fig. 40. It is evident that the composition of ternary eutectics was close to the predicted. The ternary eutectic point lies in a specific triangle, which is formed by the FeO phases and solid solutions based on UO_2(ZrO_2,FeO) and ZrO_2(UO_2,FeO) crystallized in the system (Fig. 25, points P4 and P5), and its temperature is lower than the temperature of binary eutectics in the UO_2-FeO and ZrO_2-FeO systems [7,14]. Both observations confirm the credibility of produced results.

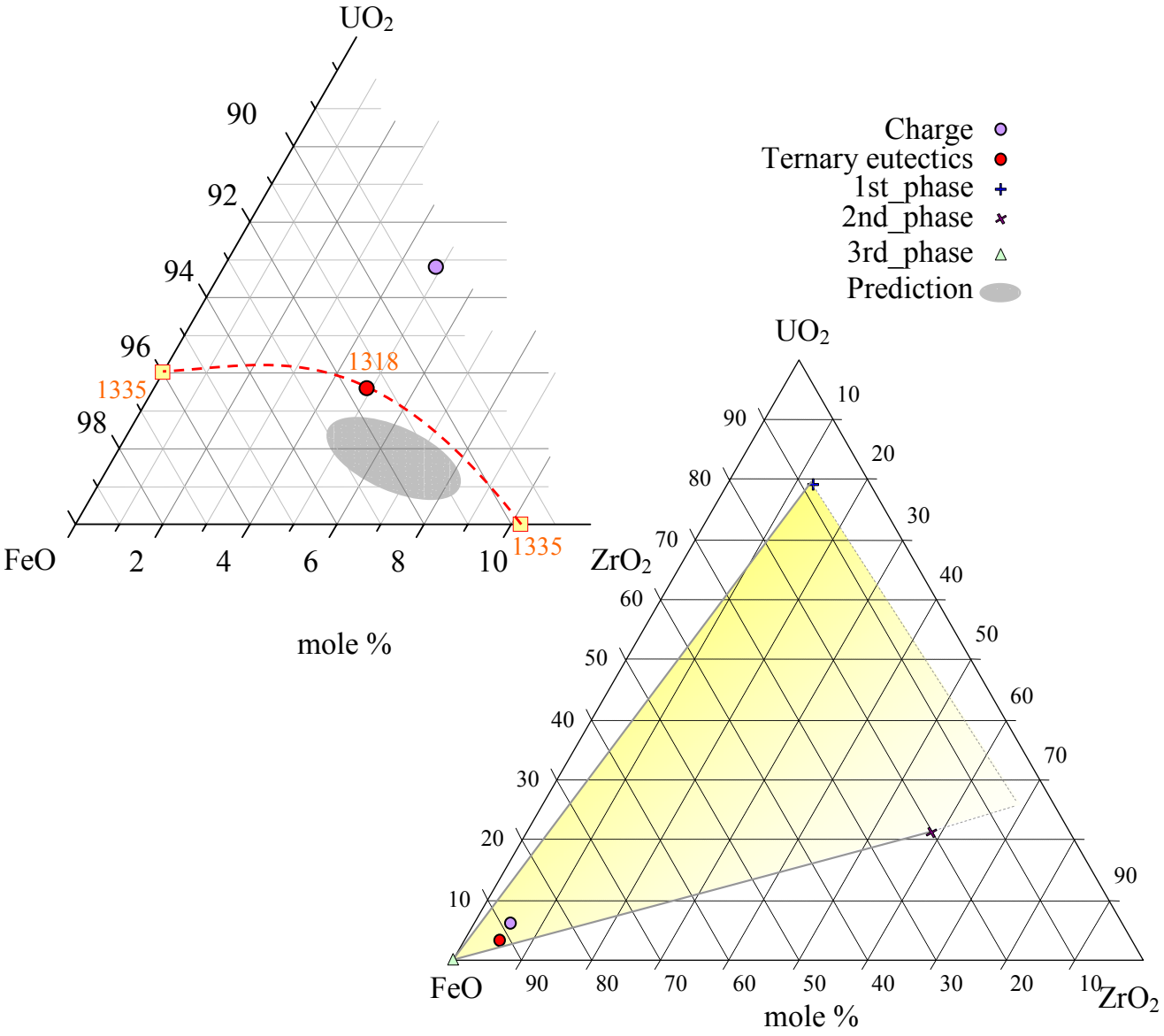

Fig. 40. Concentration triangle of the UO_2-ZrO_2-FeO system with experimental points (CORD-25, CORD-31)

Analysis of the experiment conducted in air (CORD-27) enabled to determine phase compositions (U_3O_8(ZrO_2,Fe_2O_3), U_3O_7(ZrO_2,Fe_2O_3), Fe_2O_3 and U(Zr)FeO_4) and average compositions (32 mol% UO_{2+x}, 2.1 mol% ZrO_2 and 65.9 mol% $FeO_{1.5}$) of eutectic structures. In the mass% this composition is: 61.04 mass% UO_{2+x}, 1.74 mass% ZrO_2 and 37.22 mass% Fe_2O_3.

Using DTA the solidus temperature of those structures was determined as 1339°C. After the comparison of this value with binary eutectics temperatures of UO_{2+x}-FeO_y and ZrO_2-FeO_y, which are 1349 and 1525°C, correspondingly [3,4], we can state that the resulting value is the lowest of those obtained during the investigation.

An important consideration is that the studied composition is located on the line of the liquidus surfaces crossing in the UO_{2+x}-ZrO_2-Fe_2O_3 system, which was predicted (Fig. 4).

The mentioned facts prove that the composition 32 mole% UO_{2+x}; 2.1 mole% ZrO_2 and 65.9 mole% $FeO_{1.5}$ corresponds to the ternary eutectics with crystallization temperature of 1339°C. The data are summarized in Fig. 41. The most representative of the three analyzed eutectic zones is the structure of Fig. 22, SQ2.

The following comment should be maid about the compositions of final solid solutions $U_3O_7(ZrO_2,FeO_y)$ and $U_3O_8(ZrO_2,FeO_y)$, which are included into the eutectics: a definite conclusion can be made only about one of them. The reason is that SEM/EDX method cannot separate them, because of indistinct contrast between these phases. The content of iron oxide in one of these solid solutions is 3.2 mol % (recalculated for $FeO_{1.5}$. Fig. 19, point P4).

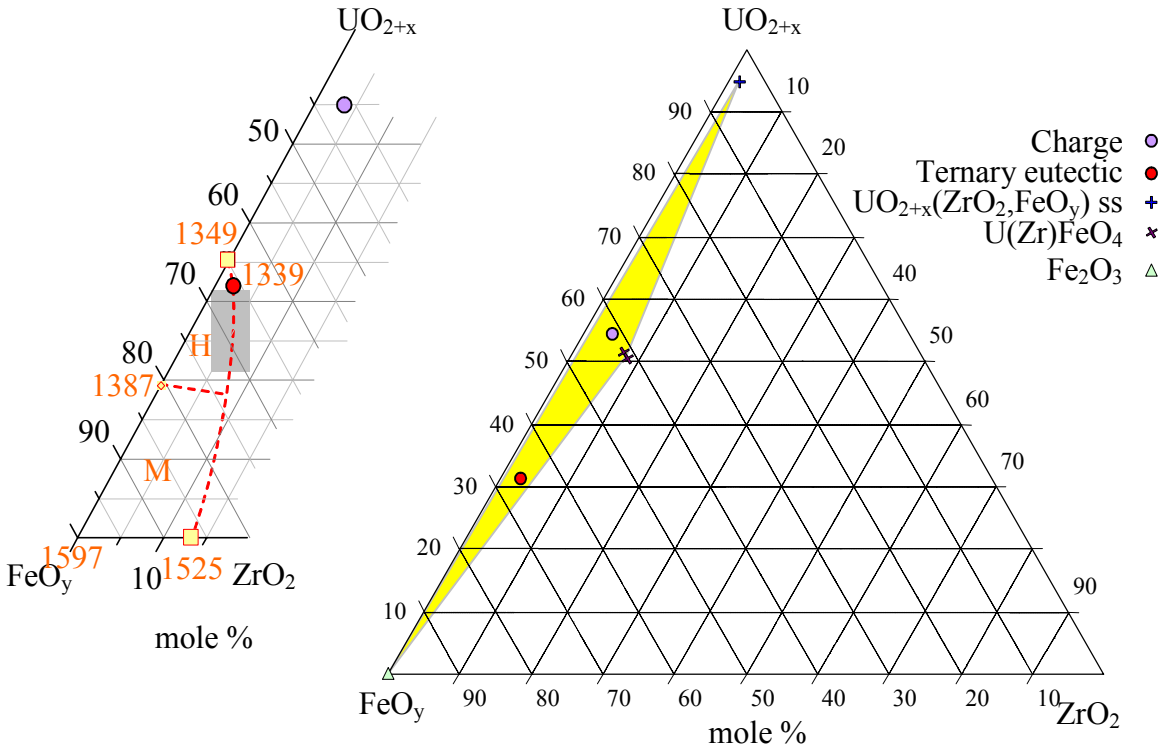

Fig. 41. Concentration triangle of the UO_{2+x}-ZrO_2-FeO_y system with experimental points (CORD-27)

5. Conclusions

- The eutectics temperature and composition have been determined for the UO_2 – ZrO_2 –FeO system in the inert atmosphere, they correspond to 3.6 mole% UO_2, 4.9 mole% ZrO_2 and 91.5 mole% FeO (11.8 mass% UO_2, 7.4 mass% ZrO_2 and 80.8 mass% FeO) and 1318±5°C.

- The final solubility of FeO in the UO_2(ZrO_2,FeO)-based phase has been determined in this system; it is 8±2 mole% (2.5±1 mass%) FeO. For a ZrO_2(UO_2,FeO)-based solid solution the final solubility of FeO can be evaluated as ~20 mole% FeO. It should be noted that due to the crystallization features of this system a lower than actual FeO solubility limit evaluation is possible, especially in the UO_2-based solid solution.

- The eutectics temperature and composition have been determined for the UO_{2+x}– ZrO_2 –$FeO_{1.5}$ system in air, which correspond to 32 mole% UO_{2+x}, 2.1 mole% ZrO_2 and 65.9 mole% $FeO_{1.5}$ (61.04 mass% UO_{2+x}, 1.74 mass% ZrO_2 and 37.22 mass% Fe_2O_3) and 1339±5°C.

- The final solubility of FeO_y in the solid solution UO_{2+x}(ZrO_2,FeO_y), has been determined as 3.2±0.8 mole% FeO_y

- Noteworthy are considerable changes in eutectic composition and temperature, as well as the final solubility of iron oxides, which follow the change of oxygen potential in the considered oxidic system.

References

1. New Experiments on the Interaction of ZrO_2 Material with Corium Melts and Phase Diagram Points in UO_2-Based Systems. CIT Project Report, Corium Interactions and Thermochemistry, In-Vessel Cluster, INV - CIT(99)-P037, December 1999.
2. Phase diagrams for multicomponent systems containing corium and products of its interaction with NPP materials (CORPHAD) ISTC Project 1950.2. Work Plan, 2003.
3. Toropov N.A. et al. Phase diagrams of the refractory oxidic systems, v. 5, p. 289 (system Fe_3O_4–UO_{2+x} – air - source Riley B. // Trans. Amer. Nucl. Soc., V.12, P. 543-544, 1969).(In Russian)
4. Toropov N.A. et al.. Phase diagrams of silicate systems. Reference book. First issue, binary systems, second revised edition, p. 468. (system Fe_3O_4–ZrO_2 – air - source Jones T.S., Sh.Kimura, A.Muan. // Journ. Amer. Ceram. Soc., 50, №3, 137, 1967). (In Russian)
5. Toropov N.A. et al. Phase diagrams of silicate systems. Reference book. First issue, binary systems, second revised edition, p. 669-672. (In Russian)
6. S.V.Bechta, V.B.Khabensky, E.V.Krushinov, S.A.Vitol, D.B.Lopukh, A.Yu.Petchenkov, A.P.Martinov, I.V.Kulagin, "Investigations of interaction of corium with zirconium dioxide concrete", Proc. of Applied Research Workshop "Safety Issues of NPP with WWER", September 12-14, 2000, St. Petersburg.
7. Investigation of binary oxidic systems. System UO_2-FeO. ISTC PROJECT № 1950.2. Annual progress report. First year, 2004.
8. Fedorov A.A. New methods of analysis of metallic powders and cinders. M.: Metallurgy, 1972. (In Russian)
9. Skug D., West D. Basics of analytical chemistry. v.1,2. M.: Mir, 1979. (In Russian)
10. Markov V.K. et al. Uranium. Methods for its detection. M.: Atomizdat, 1964. (In Russian)
11. GOST 4011-72. Drinking water. Methods for measuring mass concentration of total iron. (In Russian)
12. Sendel E. Colorimetry methods for determining traces of metals. M.: Mir, 1964. (In Russian)
13. T.M. Florence- Analytical methods in the nuclear fuel cycle/ Vienna: JAEA, 1972. 2. Methods for determining O/U in the sub-stoichiometric UO_2. Radiochemistry, v.36, issue 3, 1994. (In Russian)
14. Investigation of binary oxidic systems. System ZrO_2-FeO. ISTC PROJECT № 1950.2. Annual progress report. First year, 2004.
15. Toropov N.A. et al. Phase diagrams of the refractory oxidic systems, v. 5, p. 289 (system UO_2-Fe_3O_4-O – air - source Evans W. D. J., White J. // Trans. Brit. Ceram. Soc., V.63, N 12, P. 705-724, 1964). (In Russian)
16. Riabchikov D.I., Seniavin M.M. Analytical chemistry of uranium. M.: Ac of Sc. USSR. 1962. (In Russian)
17. Lukianov V.F., Savin S.B., Nikolskaya I.B. Photometric determination of U microquantities using reagent arsenazo III. Journal of Analytical Chemistry., XV, issue 3. 1960. (In Russian)
18. Hoekstra, H., Marshall R. // Adv. Chem. Ser., 211, 1967.
19. Tresviatsky S.G., Kushakovsky V.I. // Atomic energy. 1960. v.8, issue 1, p.56-58. (In Russian)